Basin Research

WILEY | IAS

RESEARCH ARTICLE

Non-Isochronous Transgression in Dual-Provenance Sedimentary Basins: Insights From Experimental Studies and Geometric Analysis

Wei Zhang[1,2] | Junhui Wang[1,2] | Zhuang Li[1,2] | Gesi Tao[1,2] | Li Li[1,2] | Ranran Xia[3]

[1]State Key Laboratory of Petroleum Resources and Engineering, China University of Petroleum (Beijing), Beijing, China | [2]College of Geosciences, China University of Petroleum (Beijing), Beijing, China | [3]Institute of Geology and Geophysics, Chinese Academy of Sciences, Beijing, China

Correspondence: Junhui Wang (wangjunhui@cup.edu.cn)

Received: 18 March 2025 | **Revised:** 3 January 2026 | **Accepted:** 24 January 2026

Keywords: autoretreat theory | autostratigraphy | dual-provenance system | flume experiments | transgression

ABSTRACT

In conventional sequence stratigraphy, it is commonly believed that transgression occurs simultaneously across the sedimentary basin experiencing relative sea-level (RSL) rise. As a consequence, the maximum flooding surface is widely utilised as a quasi-isochronous chronostratigraphic marker for regional stratigraphic correlation. The concept of shoreline autoretreat demonstrates that the transgression may occur after a precursory regression. How long the precursory regression would last depends on external forcings including the rate of sediment supply (q_s) and rate of RSL rise (R_{rsl}) and slope features of the basin. This means within a given basin, the onset of transgression varies in locations with different sediment supply rates and/or slope features. This study aims to analyse the influencing factors of the occurrence time of transgression in dual-provenance basins through theoretical modelling and two-dimensional flume experiments. To investigate these factors, two series of tank experiments were designed. The first series is supply-modulated where the two provenances were different in q_s, while the basin slope condition were kept the same. The second series is modulaed where the two provenances varied in hinterland slopes (γ) while q_s were kept the same. Each series included 2 or 3 runs with different multiples of R_{rsl} or q_s. Furthermore, a reference run was performed where the two provenances were identical in both q_s and γ. The results reveal that: (1) q_s and R_{rsl} have similar effect on transgression. As q_s increases, the timing of transgression is delayed, while an increase in R_{rsl} accelerates its occurrence. Both factors affect the timing of transgression by altering the size of the river-delta system. (2) The occurrence of transgression is closely related to the size of the river-delta system. Guided by the autoretreat mechanism, the fluvial-deltaic system maintains its progradational trend during a constant RSL rise, provided it has not yet reached its critical dimensions. A transgressive retreat is fundamentally postponed until the delta evolves to exceed this intrinsic spatial threshold, at which point the required sediment volume for progradation outstrips the supply. Only when the river-delta size exceeds the critical size does transgression take place. The critical size is controlled by a combination of q_s, R_{rsl}, and basin slope. (3) Hinterland slope (γ) affects subaerial and subaqueous allocations of sediment. Larger γ result in a reduction of subaerial allocations of sediment. As a result, the alluvial realm expands slower but the aggradation rate is higher, by which transgression is delayed. The Canterbury Plain in New Zealand serves as a potential example of asynchronous transgression in a basin with varying provenance. Based on an understanding of autostratigraphic processes, these findings offer a framework for explaining the anisochronicity of transgression in natural basins and provide a novel perspective for reconstructing basin evolution and stratigraphic analysis.

Highlight

1. Transgression starts when delta size exceeds a threshold set by q_s, RSL, and slope.
2. Hinterland slope governs sediment partitioning, delaying or advancing shoreline transgression.
3. Flume experiments validate models and show asynchronous retreat in dual-provenance basins.
4. Findings provide a framework to interpret non-isochronous stratigraphy and basin evolution.

1 | Introduction

Relative sea level (RSL) change, as a combination of eustasy, compaction and tectonic movement, is key to stratigraphic analyses (Mastronuzzi et al. 2005; Milne et al. 2009; Cazenave and Llovel 2010). Early sequence stratigraphic models often assumed that transgression occurred nearly synchronously across offshore depositional environments and sedimentary basins during periods of RSL rise (Johnson et al. 1985; Summerhayes 1986), thereby treating the resulting flooding surfaces as isochronous markers for regional or global stratigraphic correlation (Vail et al. 1977; Haq et al. 1987; Van Wagoner et al. 1988, 1990; Embry and Johannessen 1992). However, subsequent studies have questioned the validity of this assumption, highlighting that transgression is not a basin-wide instantaneous event but a time-transgressive process governed by local sediment dynamics and physiographic conditions (Shanley and McCabe 1994; Muto and Steel 1997; Paola et al. 2009; Gearon et al. 2022). This recognition sets the stage for alternative interpretations of stratigraphic surfaces and motivates a closer examination of the mechanisms that control transgression timing.

The concept of shoreline autoretreat suggests that, for a fluvio-deltaic system experiencing RSL rise, the transgression occurs after a precursory regression (Muto and Steel 1992). Through numerical models and flume experiments, Muto et al. have investigated the turnaround of shoreline regression to transgression (Muto and Steel 1992, 1997; Muto 2001). Their findings demonstrate that the timing of transgression is determined by the rate of sediment supply, the rate of RSL rise, and slope parameters including the topset and foreset slope, basin floor slope and hinterland slope (Muto 2001; Wang and Muto 2021). While both the timing and extent of transgression are important for understanding stratigraphic architecture, the timing of shoreline turnaround is particularly sensitive to these external forcings and governs how and when the transgressive surface is formed. In this study, we focus on the timing of transgression because it directly reflects the response dynamics of the coastal system to variations in sediment supply and basin physiography, and can be systematically tracked in flume experiments. In the autoretreat model, shoreline progradation can persist even under rising RSL, until the system reaches a point where sediment delivery becomes insufficient to expand the subaerial realm. Only after this critical point, transgression occurs. The autoretreat model is essential for understanding shoreline turnaround dynamics, but it should not be conflated with regressions primarily driven by falling and standstill stages of eustatic sea-level changes as illustrated in traditional stratigraphic sequences (Lisiecki and Raymo 2005; Thomas et al. 2020).

To date, the autostratigraphy theory has been examined mostly in a single sediment supply context (Muto et al. 2007; Wang and Muto 2021). In a sedimentary basin, sediment feeding and marginal topography vary locally. In this context, how strata are stacked up in response to the autoretreat principle has not been investigated yet. This study aims to investigate the factors influencing transgression through theoretical reasoning and two-dimensional tank experiments, particularly under steady dual-provenance conditions. In the present model, the sediment supply and RSL rise started from zero water depth in a basin with no pre-existing sediment. Our findings indicate that the onset timing of transgression is delayed by higher sediment supply rates (q_s) and steeper hinterland slopes, whereas it exhibits an inverse-square relationship with the rate of RSL rise (R_{rsl}). Importantly, the slope features of the basin also influence the stratigraphic stacking patterns during transgression.

2 | Autoretreat and Numerical Prediction

Shoreline autoretreat, probably the first formally recognised large-scale autogenic phenomenon, is defined as transgression occurring inevitably after the regressive fluvio-deltaic system has reached a specific stage, under conditions of constant RSL rise and with all other external forcings, including sediment supply, remaining steady (Muto and Okada 1991; Muto and Steel 1992, 1997; Wang et al. 2024). The process of shoreline autoretreat can be classified into two types: (i) if the hinterland slope (γ) exceeds the foreset slope (β), the fluvio-deltaic system undergoes a successive evolution comprising: progradational regression up to the autoretreat point (maximum regression), ensuing deltaic transgression (characterised by the maintenance of both topset and foreset), and ultimate autodrowning, where the entire depositional system becomes submerged (Figure 1a); (ii) if γ is shallower than β, after the fluvio-deltaic system has completed the transition from regression to transgression, it enters into a non-deltaic transgression phase after the attainment of autobreak, an event after which the foreset of the system is abandoned and sediment starved (Figure 1b, Muto 2001; Wang and Muto 2021; Wang et al. 2024).

Existing studies of autoretreat only considered a single sediment supply. In the real world, sediment supplies are from various directions into the basin. Controlled by the amount of sediment supply and local basin physiography, the process of autoretreat may proceed diachronously in fluvio-deltaic systems of different locations. In the following, we will show the diachroneity of transgressions across two provenance systems in the basin using two-dimensional geometric models and flume experiments (Figure 2).

A dual-provenance sedimentary basin system in the *X-Z* plane (where *X* represents horizontal basinward distance and *Z* represents height) is considered, with the junction point of the left hinterland and the basin floor located at (0, 0) (Figure 2). Each fluvio-deltaic depositional system is characterised by 4 surfaces and 3 moving boundaries. The 4 surfaces are the topset surface, foreset surface, basin floor, and hinterland and their slopes are

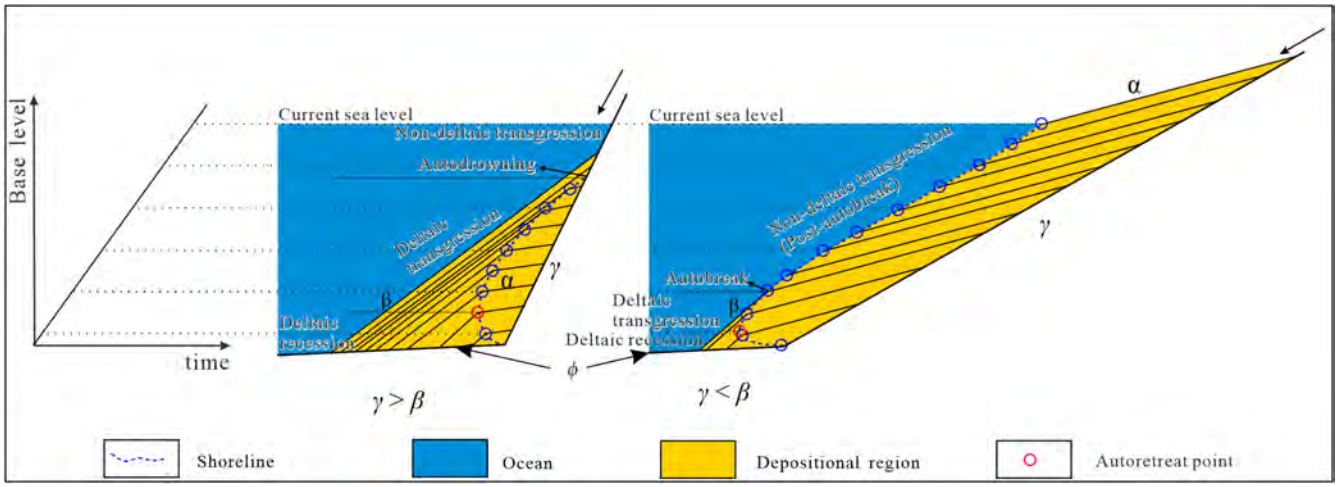

FIGURE 1 | Two-dimensional autoretreat to steady RSL rise, given a constant rate of sediment supply (Wang and Muto 2021). (a) Shoreline autoretreat and autodrowning under the slope condition $\gamma > \beta$. The growing clinoform experiences deltaic regression, then deltaic transgression, and eventually submergence (autodrowning). (b) Shoreline autoretreat and autobreak under the slope condition $\gamma < \beta$. The growing clinoform experiences deltaic regression, then deltaic transgression, followed by non-deltaic transgression (after autobreak).

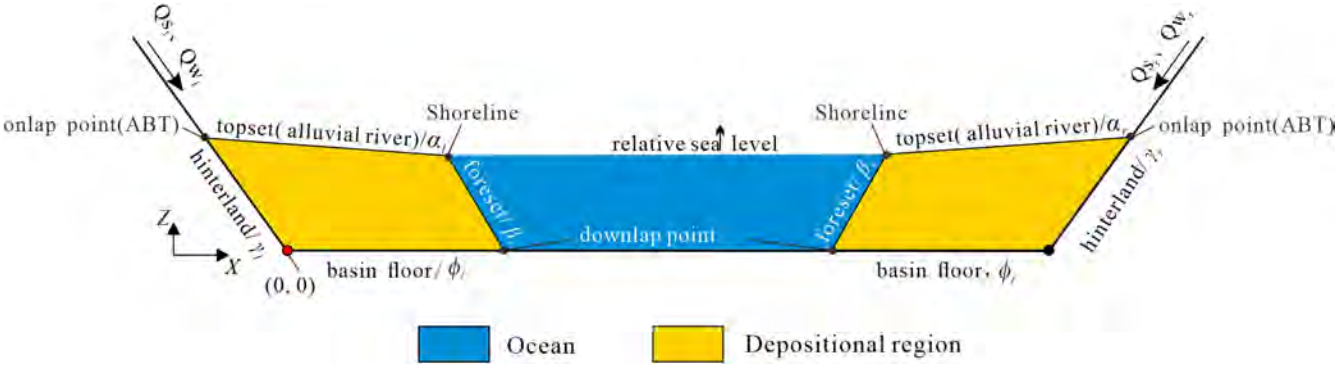

FIGURE 2 | Schematic illustration of a dual-provenance sedimentary basin growing with RSL rise. The angles α, β, ϕ and γ represent the tangent values of the slopes for the topset surface, foreset surface, basin floor, and hinterland, respectively. The subscripts 'l' and 'r' denote the two different provenance systems on the left and right sides. For example, α_l represents the slope of the topset surface in the left provenance system.

marked as α, β, ϕ, and γ, respectively. In the present study, ϕ is always set as 0, that is, a horizontal basin floor. The 3 moving boundaries are the onlap point (alluvial-basement transition, ABT), downlap point (deltaic toe), and shoreline, which were coincident at the junction point of the hinterland and basin floor at time $t = 0$. Each fluvio-deltaic depositional system is governed by characteristic length and time scales. To quantify the evolution of the system, we first define the characteristic length scale (Λ_{2D}) and time scale (τ_{2D}) as follows (Muto et al. 2007; Wang et al. 2024):

$$\Lambda_{2D} = \frac{q_s}{|R_{rsl}|} \tag{1}$$

$$\tau_{2D} = \alpha \frac{q_s}{|R_{rsl}|^2} \tag{2}$$

where q_s represents the sediment supply rate [L^2/T] and R_{rsl} represents the constant rate of relative sea-level (RSL) rise [L/T]. These scales serve as the fundamental units for the subsequent dimensionless analysis. In the model presented in Figure 2, the trajectory for shoreline autoretreat follows a theoretical curve, which is essentially the same for both the left and right provenance systems. According to the original work of Petter and Muto (2008), the theoretical shoreline autoretreat curve of the left system can be expressed as:

$$X = c_{1l} Z + \sqrt{c_{2l} Z^2 + c_{3l} \frac{q_{sl}}{|R_{rsl}|} Z}. \tag{3}$$

where c_{1l}, c_{2l}, and c_{3l} are coefficients determined by α_l, β_l, ϕ_l, γ_l, (α_l, β_l, ϕ_l and γ_l represent the slopes for the topset surface, foreset surface, basin floor, and hinterland, respectively, for the left provenance system). c_{1l}, c_{2l}, and c_{3l} are expressed as follows:

$$c_{1l} = \frac{\alpha_l \phi_l - \beta_l \gamma_l}{\alpha_l \gamma_l (\beta_l - \phi_l) + \beta_l \phi_l (\gamma_l - \alpha_l)} \tag{4a}$$

$$c_{2l} = {c_{1l}}^2 - \frac{\beta_l - \phi_l + \gamma_l - \alpha_l}{\alpha_l \gamma_l (\beta_l - \phi_l) + \beta_l \phi_l (\gamma_l - \alpha_l)} \tag{4b}$$

$$c_{3l} = \frac{2(\gamma_l - \alpha_l)(\beta_l - \phi_l)}{\alpha_l\gamma_l(\beta_l - \phi_l) + \beta_l\phi_l(\gamma_l - \alpha_l)} \tag{4c}$$

Particularly, at the autoretreat point, $dX/dZ = 0$, and the following relationship holds:

$$c_{4l}X + c_{5l}Z = \frac{q_{sl}}{|R_{rsl}|} = \Lambda_{2Dl} \tag{5}$$

where c_{4l} and c_{5l} are coefficients determined by α_l, β_l, ϕ_l, γ_l

$$c_{4l} = \frac{\beta_l\gamma_l - \alpha_l\phi_l}{(\gamma_l - \alpha_l)(\beta_l - \phi_l)} \tag{6a}$$

$$c_{5l} = \frac{\beta_l - \phi_l + \gamma_l - \alpha_l}{(\gamma_l - \alpha_l)(\beta_l - \phi_l)} \tag{6b}$$

Equation (5) shows the critical conditions for the turnaround of regression and transgression during the rise of the RSL. Basically, the shoreline trajectory expressed by Equation (3) evolves with the size change of the depositional system. That is, if the fluvio-deltaic system exceeds the scale defined by Equation (5), transgression will occur; otherwise, regression sustains.

The theoretical shoreline autoretreat curve of the right system can be expressed as:

$$X = C - \left(c_{1r}Z + \sqrt{c_{2r}Z^2 + c_{3r}\frac{q_{sl}}{|R_{rsl}|}Z}\right) \tag{7}$$

where C denotes the length of the basin floor. The coefficients c_{1r}, c_{2r}, and c_{3r} have the same mathematical forms as Equation (4a–c), but are determined by the slope parameters α_r, β_r, ϕ_r, γ_r, which represent the topset surface, foreset surface, basin floor, and hinterland for the right provenance system. At the autoretreat point, Equation (5) can be simplified as:

$$c_{4r}(C - X) + c_{5r}Z = \frac{q_{sr}}{|R_{rsl}|} = \Lambda_{2Dr} \tag{8}$$

where c_{4r} and c_{5r} take the same functional form as Equation (6a,b), but with the slope parameters of the right provenance system.

Figure 3 illustrates how the shoreline trajectory solution space, defined by $c_4X + c_5Z = \frac{q_s}{|R_{rsl}|}$, is influenced by three factors: slope parameters (c_4, c_5), q_s, and R_{rsl}. The three rows of graphs show the impact of these factors on $\frac{q_s}{|R_{rsl}|}$. The first row demonstrates how changes in slope affect the steepness of the isolines without altering their magnitude. The second row illustrates that Λ_{2D} increases with sediment supply rate, but the steepness of the isolines remains unchanged. The third row shows that as the RSL rise rate decreases, $\frac{q_{sl}}{|R_{rsl}|}$ increases, again without affecting the slope of the isolines. While slope determines the geometry of the shoreline trajectory, q_s and R_{rsl} only shift the isoline positions by scaling $\frac{q_{sl}}{|R_{rsl}|}$, influencing the timing of shoreline turnaround without changing the trajectory's shape.

The vertical position of the shoreline at the autoretreat point ($Z_{autoretreat}$) is determined by finding the stationary point of the shoreline trajectory where the rate of regressive expansion is balanced by the rate of RSL rise. By substituting the geometric coefficients from Equation (3) into the critical condition defined in Equation (5), and solving for the vertical coordinate Z, we obtain the following expression:

$$\begin{aligned} Z_{autoretreat} &= \frac{-c_{1l}c_{3l}\sqrt{c_{1l}^2 - c_{2l}} - c_{3l}(c_{1l}^2 - c_{2l})}{2c_{2l}(c_{1l}^2 - c_{2l})}\frac{q_{sl}}{|R_{rsl}|} \\ &= \frac{-c_{1l}c_{3l}\sqrt{c_{1l}^2 - c_{2l}} - c_{3l}(c_{1l}^2 - c_{2l})}{2c_{2l}(c_{1l}^2 - c_{2l})}\Lambda_{2D} \end{aligned} \tag{9}$$

This expression highlights that the maximum regressive thickness is a product of the basin's geometric configuration (represented by the coefficients c_{1l}, c_{2l}, c_{3l} and the characteristic length scale Λ_{2D}). Using the relationship between height Z and time t, which is $Z = R_{rsl} * t$, we substitute $Z_{autoretreat}$ into this equation:

$$R_{rsl} * t_{autoretreat} = \frac{-c_{1l}c_{3l}\sqrt{c_{1l}^2 - c_{2l}} - c_{3l}(c_{1l}^2 - c_{2l})}{2c_{2l}(c_{1l}^2 - c_{2l})}\frac{q_{sl}}{|R_{rsl}|} \tag{10}$$

This gives us the following expression for the time of autoretreat:

$$t_{autoretreat} = \frac{-c_{1l}c_{3l}\sqrt{c_{1l}^2 - c_{2l}} - c_{3l}(c_{1l}^2 - c_{2l})}{2c_{2l}(c_{1l}^2 - c_{2l})}\frac{q_{sl}}{|R_{rsl}|^2} \tag{11}$$

This expression reveals that the timing of the transgressive turnaround is fundamentally governed by two components: a geometric factor (the term in brackets) determined by basin slopes (α, β, ϕ, γ), and a dynamic scaling factor ($\frac{q_{sl}}{|R_{rsl}|^2}$). This explains why the duration of the precursory regression ($t < t_{autoretreat}$) is highly sensitive to the rate of RSL rise—specifically, it is inversely proportional to the square of R_{rsl}. Consequently, any spatial variation in sediment supply or local RSL rise rates will lead to a non-synchronous, or diachronous, onset of transgression across the basin. Thus, the duration of the precursory regression ($t < t_{autoretreat}$) depends on external forcings including the sediment supply rate (q_s), rate of RSL rise (R_{rsl}) and the slope features of the basin (ϕ and γ), since α and β remain nearly constant during the experiment. Any of these parameters can be different among regions even in the same basin because of variations in drainage areas and local tectonic activities. Therefore, the timing of transgression might be not synchronous in a basin. So, for systems growing under different q_s and R_{rsl} conditions, they evolve differently in space and time.

To discuss the regularity among them, we establish a non-dimensionalization framework based on the system's intrinsic scales. The physical basis for these scales is intuitive: since $Z_{autoretreat} \propto \frac{q_s}{|R_{rsl}|}$, and $Z = |R_{rsl}| \times t$, it follows that the time to reach autoretreat must scale as $t_{autoretreat} = \frac{Z_{autoretreat}}{|R_{rsl}|} \propto \frac{q_s}{|R_{rsl}|^2}$. This derivation clarifies why the characteristic time scale (τ_{2D}) involves the square of the RSL rise rate. Thus, any design or measurement with length X (or Z) and time t units becomes dimensionless by dividing by Λ_{2D} and τ_{2D}, respectively(Muto and Steel 2004, Muto et al. 2016). For example, the dimensionless vertical height $Z^* = Z/\Lambda_{2D}$, dimensionless time $t_l^* = t/\tau_{2Dl}$ (where asterisks denote dimensionless quantities in this article).

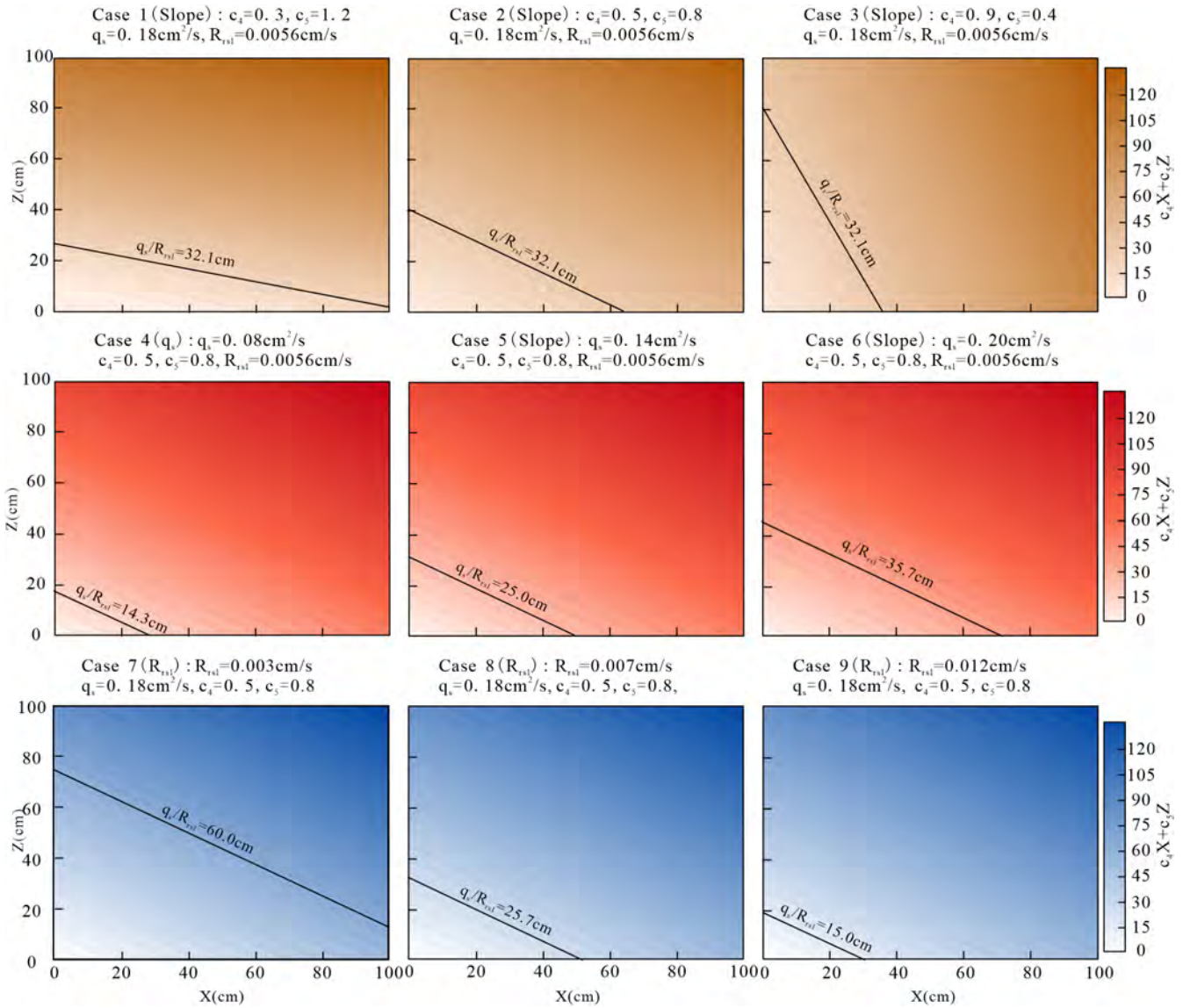

FIGURE 3 | Contour diagrams of shoreline critical condition defined by Equation (5). Row 1 (Brown): Influence of slope parameters (c_4, c_5) on shoreline shape; Row 2 (Red): Effect of sediment supply rate (q_s) on shoreline position, with shape fixed; Row 3 (Blue): Impact of RSL rise rate (R_{rsl}) on shoreline position, without altering geometry. Values are illustrative, showing the qualitative relationship described by Equation (3). Darker colours represent higher $c_4X + c_5Z$ values. Black solid lines indicate the calculated values of $c_4X + c_5Z$ for the corresponding parameters, which are labelled above each plot.

3 | Tank Experiments

The experiments were conducted at the China University of Petroleum (Beijing), using specialised facilities, including a mobile tank and a stainless steel tank measuring 2.5 m in length, 0.5 m in width, and 0.7 m in depth, equipped with a transparent glass wall for observing the longitudinal profile of dual-provenance basin transgressions (Figure 4). Inside the tank, transparent acrylic flumes of uniform 2 cm width and varying dimensions were placed (Figure 4). The narrow width of the built-in flume restricts the flow, preventing avulsion or lateral migration, and allowing only forward advancement or backward retreat. Sediment and water were supplied at constant rates from the upstream end of both sides of the flume, simulating a dual-provenance sedimentary basin system. The non-erodible flume floor consists of a downstream horizontal section (slope $\phi = 0$) representing the initial basin floor and two inclined sections representing the hinterland basement (slope γ, Figure 4). A bottom plate opening in the flume maintained water levels consistent with those in the tank, establishing the experimental RSL. The RSL was raised by adding water to the mobile tank via a PC-controlled electromagnetic flowmeter.

As previously mentioned, the timing of the transgression depends on rates of sediment supply, slope features, and RSL rise rate. In our experiments, the imposed RSL rise is treated as an external boundary condition representing eustatic sea-level change, rather than an autogenic product of shoreline dynamics (e.g., autoretreat). To test this hypothesis, a reference experiment and two different series of experiments were designed. The first series was the supply-modulated experiments, which investigated differences in the occurrence of transgression under identical basin slope conditions by varying q_s and R_{rsl} between different provenance directions. The second series was the slope-modulated

experiments, which examined the role of γ in controlling transgression by maintaining the same sediment supply rate for different provenances but altering their slope conditions. Furthermore, a reference run was performed in which the two provenances were identical in both q_s and γ, providing a baseline for comparison with the modulation experiments. Tectonic forces, such as differential subsidence and tilting, were excluded for simplicity, with base level effectively treated as equivalent to RSL in this model. The sediment used was uniform natural quartz sand (D50 = 0.52 mm) with a bulk density of 1.53 g/cm^3.

The reference run was conducted in the flume shown in Figure 4a. Both the left and right hinterland inclined to the basinward with the same slope ($\gamma_l = \gamma_r = 5.67$). Sediment supply rates from both sides were the same ($q_{sl} = q_{sr} = 0.18\,cm^2/s$, in per unit width). The RSL rose from 0 water depth at the rate of 0.0056 cm/s (R_{rsl}). No deposits existed at the beginning of the experiment.

The supply-modulated series was conducted in the same flume as that of the reference (Figure 4a) where both hinterlands had identical slope characteristics ($\gamma_l = \gamma_r = 5.67$, Table 1). Two runs were performed in this series, marked as F-1 and F-2. In run F-1, the RSL rose at the same rate as in the reference run ($R_{rsl} = 0.0056$ cm/s). The left-side sediment supply rate was kept unchanged ($q_{sl} = 0.18\,cm^2/s$), whereas the right-side supply rate was reduced to 0.09 cm^2/s ($q_{sl} = 0.18\,cm^2/s$, $q_{sr} = 0.09\,cm^2/s$). In run F-2, the sediment supply rates remained the same as in run F-1 ($q_{sl} = 0.18\,cm^2/s$, $q_{sr} = 0.09\,cm^2/s$), while the RSL rise rate was 0.0112 cm/s.

The slope-modulated series conducted in a different flume (Figure 4b), in which the left hinterland was gently inclined while the right hinterland was steeply inclined. In the present study, the definition of "steep" and "gentle" was set by the foreset slope (β) because the comparison between γ and β differentiates the autoretreat pattern. Based on the observation at the experiment, β approximated 0.74, reflecting the subaqueous angle of repose of the experimental sediment. Accordingly, we selected the gentle and steep hinterland slope at 0.58 and 5.67, respectively. In run S-1, the supply conditions were the same as in the reference run ($q_{sl} = q_{sr} = 0.18\,cm^2/s$, $R_{rsl} = 0.0056$ cm/s). In run S-2, the sediment supply rate from both the left- and right-source systems is 0.09 cm^2/s, while the RSL rise rate remained at 0.0056 cm/s. In run S-3, the sediment supply rate from both sides was kept at 0.18 cm^2/s. The RSL rose from 0 water depth at the rate of 0.0112 cm/s.

All controlling factors including RSL rise rate (R_{rsl}), sediment supply rate per unit width (q_s) and upstream water discharge (q_w) were maintained constant during each experiment. The

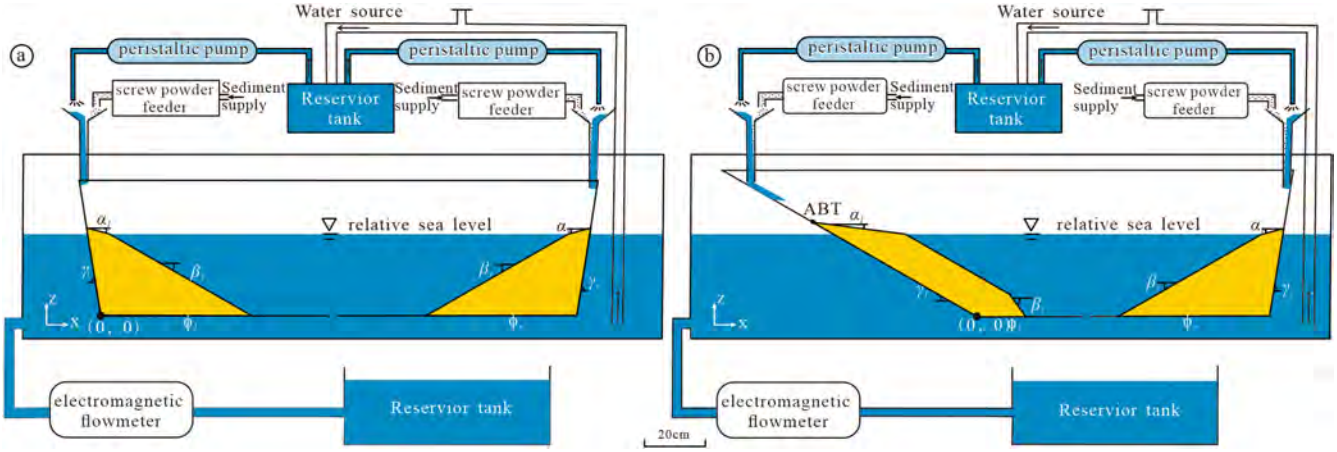

FIGURE 4 | Schematic view of the experimental set-up. (a) Detailed drawing of the experimental flume with identical hinterland slopes. (b) Detailed drawing of the experimental flume with varying hinterland slopes.

TABLE 1 | Experiments parameters.

Experiments name	Left source			Right source			R_{rsl} (cm/s)
	γ_l	q_{lw} (cm^2/s)	q_{ls} (cm^2/s)	γ_r	q_{rw} (cm^2/s)	q_{rs} (cm^2/s)	
Ref.	5.67	6.14	0.18	5.67	6.14	0.18	0.0056
F-1	5.67	6.14	0.18	5.67	3.07	0.09	0.0056
F-2		6.14	0.18		3.07	0.09	0.0112
S-1	0.58	6.14	0.18	5.67	6.14	0.18	0.0056
S-2		3.07	0.09		3.07	0.09	0.0056
S-3		6.14	0.18		6.14	0.18	0.0112

Note: q_{lw}, q_{ls}: left-side water and sediment supply rates per unit width; q_{rw}, q_{rs}: right-side water and sediment supply rates per unit width; γ_l, γ_r: hinterland slopes of the left and right sides; R_{rsl}: the relative sea-level rise rate.

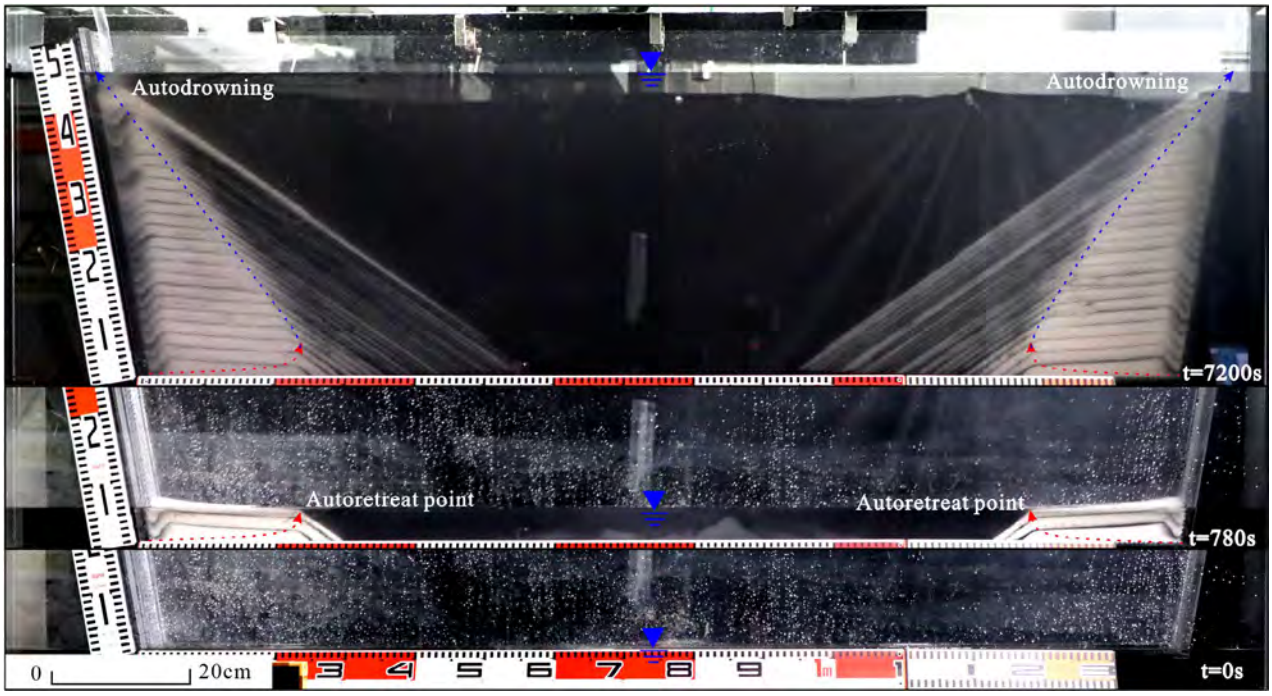

FIGURE 5 | Sequential images recorded in the reference run. Note that progradation during the first 780 s was followed by transgression in the different fluvio-deltaic systems within the basin. (The red lines represent the tracks of regressive shorelines, while the blue lines illustrate transgressive movements.)

values of R_{rsl}, q_s, and q_w were controlled by an electromagnetic flowmeter (potential error: 1%), screw feeders (p.e.: 2%), and tubing pumps (p.e.: 0.5%), respectively. In all experiments, the q_w/q_s ratio was kept constant to maintain a consistent α value. A digital camera captured images and recorded data every 30 s. A small amount of coal was added from the upstream funnel at regular intervals (4 min for runs S-1 and S-3, 5 min for the other runs) to serve as a timeline marker.

4 | Results

4.1 | Reference Experiment

Figure 5 shows the basin sedimentary system obtained from reference run. During the experiment, the variation in the alluvial slope (α) and foreset slope (β) is minimal. The average value of the alluvial slope (α) is 0.055, while the average foreset slope(β) is 0.74. The characteristic length scales of the left and right sources are $\Lambda_{2Dl}=\Lambda_{2Dr}=32.14$ cm, with corresponding time scales $\tau_{2Dl}=\tau_{2Dr}=315.69$ s (Equations 9 and 10).

The same coordinate system was used to record the sedimentary processes in the experiments as was used for the numerical analysis. At $t=0$ s, the initial river length (L_0) in both supply systems was 0, with the RSL positioned at the flume bottom ($Z=0$). Three movable boundaries, that is, the ABT, shoreline and downlap point, were initially positioned at (0,0) and (150, 0) for the left and right source systems, respectively. Soon after the run began, a fluvio-deltaic system took shape in the basin, with the shorelines on both sides rapidly migrating seaward (Figure 5). Sediment supplied from upstream primarily contributed to aggradation of the river system, while the excess sediment bypassed the shoreline and was deposited further offshore. As the progradation continued, its rate decreased. At $t=780$ s ($t_l^*=t_r^*=2.47$), the progradation rate reached zero, and the shorelines of both the left and right depositional systems reached the autoretreat point. At the autoretreat point, the river length in the left source system was 21.98 cm ($L_l^*=0.68$), and in the right system, it was 21.83 cm ($L_r^*=0.68$). As the RSL continued to rise, the left and right shorelines began retreating landward, initiating transgression. Due to the shortening of river length, a greater proportion of sediment input from upstream was deposited in the foreset. Until $t=7200$ s ($t_l^*=t_r^*=22.81$), the river length reduced to 0, with all sediment deposited subaqueously—a phenomenon known as autodrowning (Tomer and Muto 2010; Tomer et al. 2011).

Based on the measured angles α and β, the transgressions of the left and right sedimentary systems in the numerical prediction of the geometric model occurred at $Z=4.47$ cm and $t=798.32$ s ($Z^*=0.14$, $t_l^*=t_r^*=2.53$, Equations (7) and (8)), which were in good agreement with the results from the flume experiment.

4.2 | The Supply-Modulated Series

Two runs (F-1 and F-2) were conducted in this series to be compared to the reference run described above. In each experiment, the slope of the basin hinterland at both sides remained consistent ($\gamma_l=\gamma_r=5.67$). Compared to the reference run, in run F-1, the sediment supply rate from the right source was halved while that from the left source was the same. In run F-2, the same supply conditions were adopted as those of run F-1, except that the RSL rise rate was doubled.

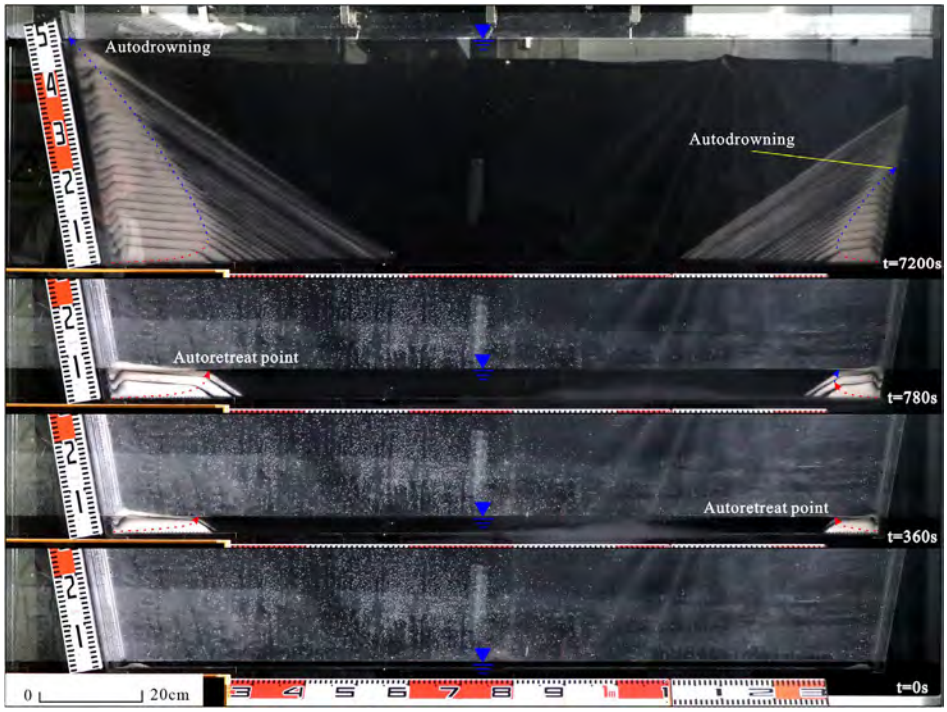

FIGURE 6 | Sequential images recorded in run F-1. Note that transgression in the left provenance occurred at 780 s, while in the right provenance, it occurred at 360 s.

In run F-1, because of the difference in q_s, the characteristic length scales of the left- and right-sourced systems were unequal, which were $\Lambda_{2Dl} = 32.14$ cm and $\Lambda_{2Dr} = 16.07$ cm, respectively. Correspondingly, the time scales of the two systems were unequal too, which were $\tau_{2Dl} = 315.69$ s (left-sourced system) and $\tau_{2Dr} = 157.84$ s (right-sourced system), respectively. For the right system, the autoretreat point was reached at $t = 360$ s ($t_r{}^* = 2.28$), and the alluvial river length reached a length of 8.27 cm ($L_r{}^* = 0.51$) (Figure 6). Afterward, transgression took place. By $t = 3600$ s ($t_r{}^* = 22.81$), the alluvial-river length became zero, and all sediment was deposited subaqueously. For the left system, the autoretreat point was reached at $t = 780$ s ($t_l{}^* = 2.47$) with the alluvial river length at 18.77 cm ($L_l{}^* = 0.58$). Compared to the right system, the timing of the attainment of the autoretreat point was 420 s delayed, with a much longer alluvial-river length. Both the timing and alluvial length were approximately doubled compared to those of the right-sourced system. Nevertheless, in the dimensionless space, the timing and alluvial-river length at the autoretreat point were 2.47 and 0.58, respectively, both of which were equivalent to those of the right-sourced system. Similarly, the autodrowning of the left-sourced system occurred at $t = 7200$ s, which was 3600 s delayed or doubled but was equivalent in the dimensionless form ($t_r{}^* = 22.81$) as compared to the right-sourced system. In the numerical prediction based on Equation (7) and (8), the onset of transgression of the left- and right-sourced systems occurred at $t = 798.32$ s and 399.16 s, respectively, both of which equaled 2.53 after normalisation with the corresponding τ_{2D}.

In run F-2, the characteristic length scales of the left and right sources were $\Lambda_{2Dl} = 16.07$ cm and $\Lambda_{2Dr} = 8.04$ cm, with corresponding time scales $\tau_{2Dl} = 78.92$ s and $\tau_{2Dr} = 39.46$ s, respectively. Both sides experienced a faster and smaller-scale autoretreat process compared to run F-1 as described below. For the right-sourced system, autoretreat occurred at $t = 90$ s ($t_r{}^* = 2.28$) when the alluvial-river length reached the length 7.6 cm ($L_r{}^* = 0.95$). Autodrowning occurred at $t = 900$ s ($t_r{}^* = 22.81$) in the right system, and all sediment was deposited underwater. For the left-sourced system, autoretreat occurred at $t = 180$ s ($t_l{}^* = 2.28$) with the alluvial length 13.60 cm ($L_l{}^* = 0.85$), and autodrowning occurred at $t = 1800$ s ($t_l{}^* = 22.81$). Therefore, similar to run F-1, the autoretreat process of the left-sourced system was approximately doubled to that of the right-sourced system, but was equivalent after normalisation with their corresponding length and time scales. In the numerical prediction, transgression in the right-sourced system occurred at $t = 99.79$ s ($t_r{}^* = 2.53$) and in the left-sourced system at $t = 199.58$ s ($t_l{}^* = 2.53$), closely matching the results of the flume experiment.

Under the influence of sediment supply rate and RSL rise rate, there are differences in the timing and spatial scales of transgression and autodrowning on both sides of the sedimentary system during the first supply modulation. In run F-1, the sediment supply on the left source is twice that on the right, and the timing of transgression and autodrowning on the left is also doubled. In contrast, in run F-2, when the RSL rise rate is doubled, the heights at which transgression and autodrowning occur are halved, and the time required is shortened to a quarter. We also note that when comparing the right-sourced system in run F-1 and the left-sourced system in run F2: while both systems shared the same length scales, the time scale of the former was nearly twice that of the latter. the autoretreat process of the former exhibited nearly identical dimensional characteristics to the latter, yet progressed at half the rate of the latter. Despite these differences in real-scale behaviour, when normalised to their respective dimensionless time and spatial scales, the timing and spatial extents of autotreat and autodrowning in the sedimentary system are highly consistent ($t^* = 2.28$–2.47),

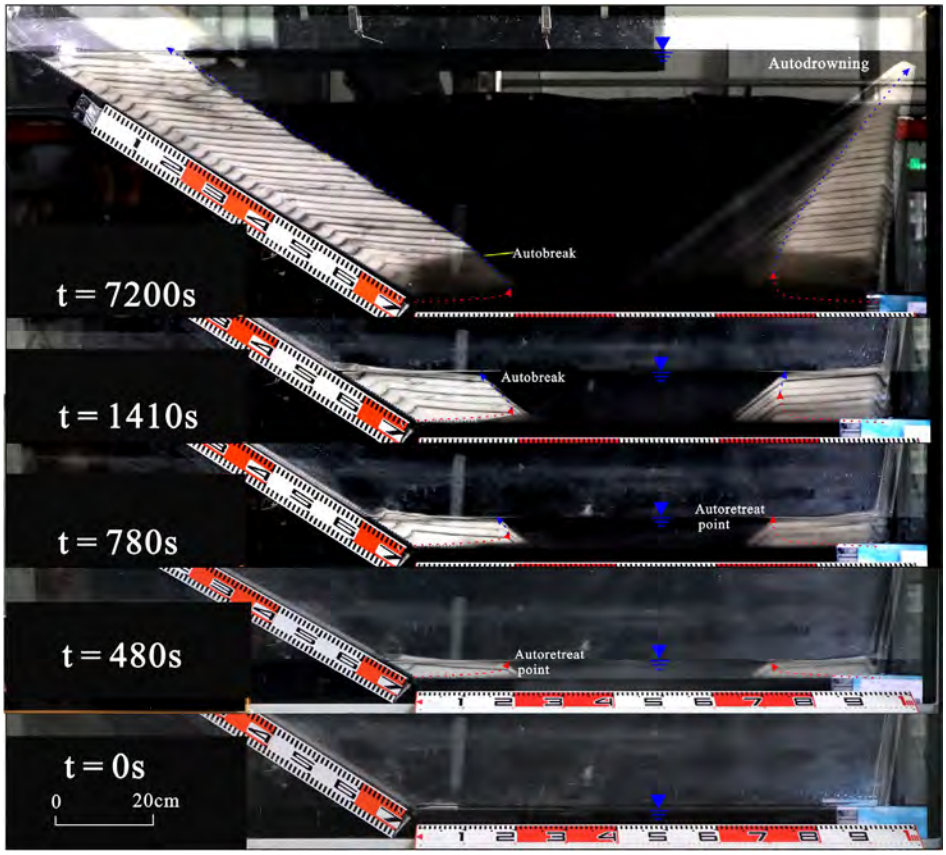

FIGURE 7 | Sequential images recorded in run S-1. Note that transgression in the left provenance occurred at 480 s, while in the right provenance, it occurred at 780 s.

closely aligning with the time and spatial scales observed in the reference run ($t^* = 2.47$). These observations reveal that the autoretreat process of a particular system is governed by specific characteristic length and time scales.

4.3 | The Slope-Modulated Series

The slope-modulated series comprise three runs, that is, S-1, S-2, and S-3. In these runs, the slopes of the left and right sources differed ($\gamma_l = 0.58$, $\gamma_r = 5.67$), while the sediment supply rate remained the same for both sources ($q_{sl} = q_{sr}$) but might be different among runs. So, in each run, the characteristic length scale and time scale of the left- and right- sourced systems were equal ($\Lambda_{2Dl} = \Lambda_{2Dr}$, $\tau_{2Dl} = \tau_{2Dr}$). In run S-1, all other experimental parameters were the same as the reference run to investigate the impact of slope on the timing of transgression. Runs S-2 and S-3 were derived based on run S-1. In run S-2, the sediment supply rates on both sides were halved from that in run S-1, while all other conditions remained unchanged compared to run S-1. In run S-3, only the RSL rise rate was changed, which was doubled to that adopted in run S-1. The coordinate system is defined in the same way as before, but the initial coordinate of the right-sourced system was positioned at (90, 0). This is because the basin floor length has changed to adjust to a gentler left hinterland basement.

In run S-1, the characteristic length scale Λ_{2D} was calculated as 32.14 cm (i.e., $\Lambda_{2Dl} = \Lambda_{2Dr} = 32.14$ cm). With a measurement of α, the characteristic time scale τ_{2D} was further calculated as 315.69 s (i.e., $\tau_{2Dl} = \tau_{2Dr} = 315.69$ s). For the right steep-slope system, the shoreline reached the autoretreat point at $t = 780$ s ($t_r^* = 2.47$), with the alluvial river length reaching a maximum of $L = 21.85$ cm ($L_r^* = 0.68$). Afterward, transgression was initiated and sustained. Until $t = 7200$ s ($t_r^* = 22.81$), the right-sourced system reached the state of autodrowning. For the left gentle-slope system, the autoretreat point was attained at $t = 480$ s ($t_l^* = 1.52$, Figure 7) with an alluvial-river length of 23.26 cm. Afterward, transgression took place. Despite the shoreline migrating landward, the sediment was supplied subaqueously to feed the foreset, and the alluvial river kept lengthening. Until $t = 1410$ s ($t_l^* = 4.47$), the sediment ceased to feed the foreset so that the foreset became sediment-starved, indicating the attainment of autobreak (Muto 2001). At this time, the alluvial river reached a critical length of $L_l = 27.32$ cm ($L_l^* = 0.85$). After the attainment of autobreak, the alluvial river length never changed, and the shoreline trajectory exhibited a linear pattern that paralleled the hinterland basement. Compared to the right steep-slope system, the left gentle-slope system finally reached the state of autobreak rather than autodrowning. Moreover, the autoretreat point attained in the left gentle-slope system was advanced, both in real scale (480 s) and dimensionless framework (1.52). In addition, the alluvial river length at the autoretreat point for the left system was 1.00 cm smaller than the right system in real scale and 0.03 larger in the dimensionless framework. Such results from the flume experiments were well captured by the numerical prediction, in which transgression in the right steep-slope system

at $t = 798.32$ s ($t_r^* = 2.53$) with alluvial river length 25.82 cm (0.80), and in the left gentle-slope system occurred at $t = 492.18$ s ($t_l^* = 1.56$) with alluvial river length 28.35 cm (0.88).

In run S-2, the characteristic length scale Λ_{2D} was calculated as 16.07 cm (i.e., $\Lambda_{2Dl} = \Lambda_{2Dr} = 16.07$ cm), and the characteristic time scale τ_{2D} was estimated as 157.84 s (i.e., $\tau_{2Dl} = \tau_{2Dr} = 157.84$ s). Both the length and time scales were halved from those in run S-1 because of the halved sediment supply. For the right steep-slope system, the system eventually evolved into the autodrowning phase as in run S-1. Specifically, the shoreline reached its autoretreat point at $t = 390$ s ($t_r^* = 2.47$), with the alluvial-river length measuring 11.12 cm ($L_r^* = 0.69$), and autodrowning at $t = 3600$ s ($t_r^* = 22.81$). For the left gentle-slope system, the timing of autoretreat and autobreak was attained at $t = 270$ s ($t_l^* = 1.71$) and 690 s ($t_l^* = 4.37$), respectively, with the alluvial-river length at 9.34 cm ($L_l^* = 0.58$) for the former and 12.67 cm ($L_l^* = 0.79$) for the latter. By comparison, the autoretreat point attained in the left gentle-slope system was advanced by 120 s in real scale and 0.76 in dimensionless framework compared to that in the right steep-slope system. For the alluvial river length at the autoretreat point, the left gentle-slope system was 1.78 cm smaller in real scale and 0.11 smaller in dimensionless value compared to the right steep-slope system. In the experiment, the alluvial river length in the right steep-slope system was longer, while in the left gentle-slope system it was shorter, whereas in the numerical simulation, the length of the alluvial river was reversed. This discrepancy could be attributed to experimental error. Such differences were also captured by the numerical simulation, which illustrated that transgression in the left gentle-slope system started at $t = 246.09$ s ($t_l^* = 1.56$) until the alluvial river reached a length 14.17 cm (0.88), and in the right steep-slope system, the corresponding timing and alluvial river length were 399.16 s ($t_r^* = 2.53$) and 12.91 cm (0.80), respectively.

In run S-3, the rate of RSL rise was doubled to that of run S-1, so that the characteristic length scale Λ_{2D} was halved to 16.07 cm (i.e., $\Lambda_{2Dl} = \Lambda_{2Dr} = 16.07$ cm), and the characteristic time scale τ_{2D} was reduced to a quarter that of run S-1 (i.e., $\tau_{2Dl} = \tau_{2Dr} = 78.92$ s). For the right steep-slope system, the shoreline reached its autoretreat point at $t = 270$ s ($t_r^* = 3.42$), with the alluvial river length reaching a maximum of $L_r = 11.80$ cm ($L_r^* = 0.73$). By $t = 1620$ s ($t_r^* = 20.53$), autodrowning was attained. For the left gentle-slope system, the shoreline reached its autoretreat point at $t = 210$ s ($t_l^* = 2.66$) at the alluvial river length of 12.67 cm (0.79). Autobreak was attained by $t = 390$ s ($t_l^* = 4.94$), at which point the river reached the critical length of $L_l = 13.97$ cm ($L_l^* = 0.87$). The transgression timing of the left gentle-slope system was advanced by 30 s in real time and 0.38 in dimensionless time compared to the right steep-slope system. The alluvial river length at the autoretreat point in the right steep-slope system was 1.16 cm smaller and 0.07 smaller in real and dimensionless lengths, respectively, compared to those in the left gentle-slope system. In the numerical simulation, transgression in the left system occurred at $t = 123.05$ s ($t_l^* = 1.56$) with an alluvial river length of 14.17 cm (0.88), and in the right at $t = 199.11$ s ($t_r^* = 2.53$) in time and 12.91 cm (0.80) in alluvial length. Although there is some discrepancy with the flume experiment results, the trend of earlier transgression on the gentle slope than on the steep slope remains consistent.

We also compared the autoretreat processes in runs S-2 and S-3, which share the same length scale, though the time scale of the former is nearly double that of the latter. This comparison shows that while the systems from both runs are equivalent in spatial scale (at real scale), the former requires approximately twice the time to reach a comparable stage. Thus, despite these real-scale differences, they are equivalent within the dimensionless framework.

Based on the results of the three runs in the second slope-modulation series, it is ascertained that the timing of transgression and autodrowning in the sedimentary system developed in gentle hinterland slope settings occurs earlier than that from steep hinterland slope settings. This difference remains even in a normalized dimensionless framework.

5 | Discussion

The comparison of the 12 shoreline trajectories from 6 runs reveals that different sediment supply rates, RSL rise rates, and slope conditions lead to a variation in the timing of the autoretreat process and thus transgression (Figure 8a). Here, RSL rise is treated as an external boundary condition representing eustatic sea-level change, rather than an autogenic response resulting from shoreline dynamics. After non-dimensionalization, the timing of transgression is the same for sedimentary systems with the same slope conditions (Figure 8b). However, this does not hold for systems evolving in different slope settings. This conclusion is consistent with the autoretreat theory, which states that the shape of the theoretical shoreline retreat trajectory is independent of changes in sediment supply rate and RSL rise rate, but is related to the slope parameters (Muto and Steel 1997).

5.1 | Effects of Sediment Supply and RSL Rise

The impact of sediment supply rate on transgression is intuitive. In the reference run, where both hinterland slope and sediment supply rate are consistent, the timing of transgression and the overall evolution of both systems were synchronous (Figure 9a). In run F-1, the sediment supply rate from the left-side source is double that of the right-side. For the left-supplied system, both the initiation time of transgression and the corresponding river length are double those observed in the right-supplied system (Figure 9b). Specifically, the sediment supply rate (q_s) exhibits a linear scaling with both temporal and spatial dimensions. As a result, the ratio of transgression timing and the relative size of the fluvio-deltaic system at the onset of transgression are directly proportional to the ratio of sediment supply rate between the two provenances.

In terms of RSL change, a similar scaling relationship is observed, but with a key distinction: the rate of relative sea-level rise (R_{rsl}) exerts a linear influence on spatial (length) scales, while its impact on temporal scales is quadratic. The rate of RSL rise also plays a key role in determining transgression timing. In comparison with run F-1, the RSL rise rate in run F-2 is doubled. In run F-2, the transgression initiation time and autodrowning time of the left-side provenance are one-fourth of that observed in run F-1, and the river length at the onset of transgression is

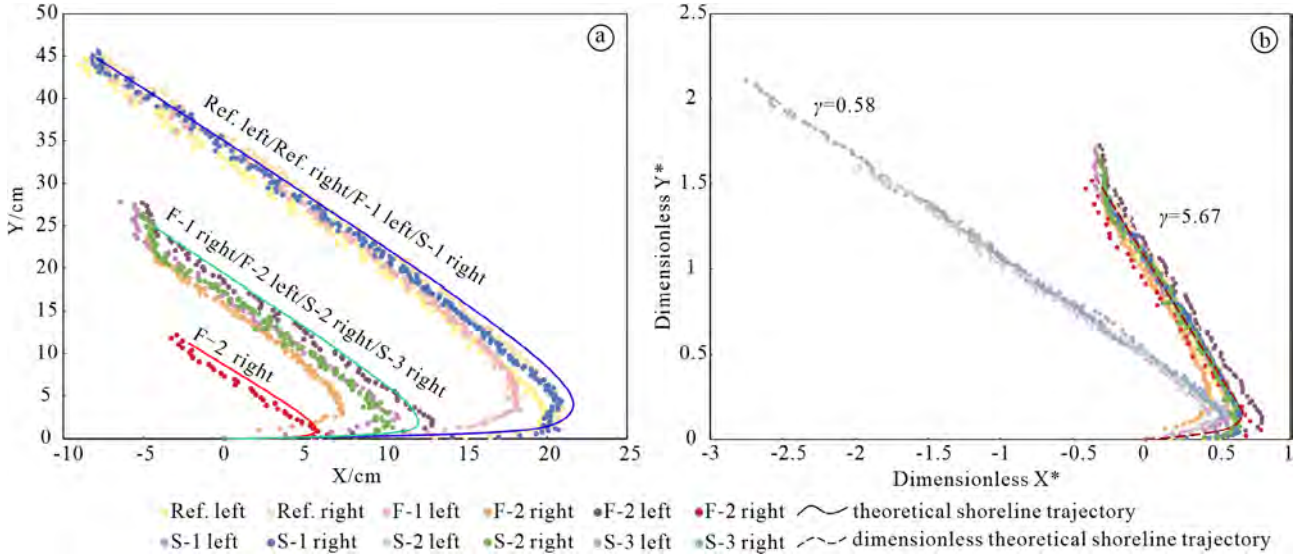

FIGURE 8 | Comparison of Shoreline Trajectory Trends. (a) Shoreline trajectories of the steep hinterland at real scale; (b) Dimensionless shoreline trajectories (The right-side shoreline trajectory is mirrored and shifted to the origin).

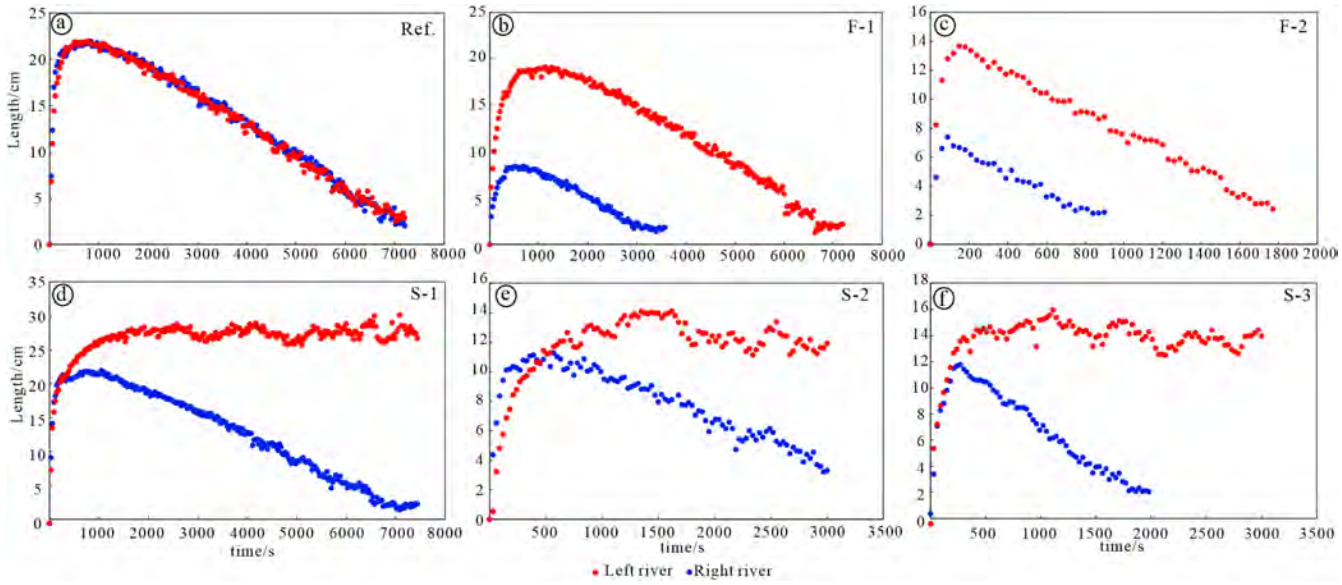

FIGURE 9 | Temporal evolution of river length in response to relative sea-level change. River length variation over time in six runs: (a) Ref., (b) F-1, (c) F-2, (d) S-1, (e) S-2, and (f) S-3. Each plot shows the evolution of left (red) and right (blue) river lengths, corresponding to two provenance directions. These diagrams illustrate how different sediment supply rates, RSL rise rates, and slope configurations affect the timing of transgression and river-delta development. The difference in river length between the left and right reflects the asynchronous transgression under dual-provenance conditions.

halved compared to that in run F-1 for the left-side provenance. The fluvio-deltaic scale development at the point of transgression is reduced by half (Figure 9c). This pattern is also observed for the right-side provenance, where the timing of transgression initiation and corresponding river length confirm this trend. The difference in transgression timing between the two provenance directions in run F-2 is also reduced to one-quarter. These results suggest that the RSL rise rate is critical for transgression, significantly influencing the timing of transgression initiation, thereby contributing to the asynchronous nature of transgression across the basin.

After non-dimensionalization using characteristic length (Λ_{2D}) and time scales (τ_{2D}), these trajectories collapse to a similar form, indicating identical shape regardless of absolute rates (Figure 8b). This scaling invariance demonstrates that sediment supply and RSL rise influence transgression through scale-dependent dynamics rather than altering the fundamental transgressive sequence. Previous studies have qualitatively established that rapid RSL rise promotes transgression, while high sediment supply can delay its onset (Le Hooke and Rohrer 1979; Zhong 2008; Van De Lageweg and Slangen 2017). Our findings highlight a more specific mechanism: transgression initiates only when the fluvio-deltaic system exceeds a critical spatial scale jointly controlled by q_s and R_{rsl}. In multi-provenance basins, this threshold-based behaviour leads to asynchronous transgression between sub-basins. Notably, autogenic processes—particularly shoreline autoretreat—can shape

key stratigraphic surfaces such as maximum flooding surfaces. Although concave shoreline trajectories are often attributed to accelerating RSL rise or sediment starvation, our results show that similar geometries can emerge under linear RSL rise and steady sediment supply, challenging conventional interpretations based solely on external forcing.

5.2 | Effects of Slope Features of the Hinterland Basement

Previous studies (e.g., Muto and Steel 1992; Wang et al. 2020; Wang and Muto 2021) have shown that hinterland slope exerts strong control over shoreline stacking patterns during transgression. For example, in steeper hinterland settings, only foresets develop during the late stage, whereas in gentler hinterland settings, only topsets are formed. (as described in Section 1). However, the effect of slope on transgression timing is seldom discussed. In the slope-modulated series, hinterland slope was the only variable, while sediment supply rate and RSL rise rate remained constant across different supply directions in each run. According to this series of runs, in gentler hinterland slope settings, transgression occurs earlier, with shorter alluvial river lengths at the onset of transgression (Figure 9d–f). Unlike the impact of sediment supply rate and RSL rise rate, there is no obvious proportional relationship between the hinterland slope and transgression initiation time and river length. Moreover, the impact of hinterland slope is reflected not only in real scale but also the normalised dimensionless framework. For example, for the steeper slope, the dimensionless transgression initiation time was $t^*=1.99$; for the gentler slope, $t^*=1.22$. This occurs because the hinterland slope fundamentally governs the sediment partitioning between subaerial and subaqueous domains, thereby defining the geometric framework of shoreline trajectories (Figure 9b). In contrast, variations in sediment supply and RSL rise primarily dictate the spatio-temporal scale and the timing of the transgressive transition, rather than reconfiguring the intrinsic geometric path of the trajectory.

The effect of hinterland slope on transgression is reflected in the differences in sediment distribution. Under the influence of RSL rise, different hinterland slopes give rise to different landward migration rates of the ABT. The gentler the slope, the faster the river extends upstream. As a result, the alluvial river expands faster so that the topset is more capable of accommodating sediment and thus less sediment is delivered beyond the shoreline (Figure 10). Consequently, the seaward advance of the shoreline is suppressed so that transgression takes place earlier. In contrast, when the hinterland slope is steeper, transgression is delayed.

Natural delta foreset slopes are generally less steep than those created in laboratory experiments, as they are shaped by wave action and sediment characteristics. Subaerial delta-front slopes typically range from 2° to 6°, while subaqueous slopes are often around 0.5°–2° (Patruno et al. 2015; Rey et al. 2022; Osman et al. 2024; Steel et al. 2024). However, both of these are still steeper than the slope of the hinterland (delta plain), which is typically much gentler, ranging from 0.01° to 0.1° (Patruno et al. 2015). Thus, in most natural environments, the foreset slope tends to be steeper than the hinterland slope. Relatively steep hinterland slopes, such as those found in foreland basins, intracratonic river basins and rift-related tectonic settings, provide valuable opportunities to explore the influence of slope on transgression. In rift basins, where both steep and gentle slopes coexist, the impact of hinterland slope on shoreline trajectory during transgression or lake transgression becomes particularly pronounced, affecting the migration patterns across different provenance directions (Withjack et al. 2002; Tomer et al. 2011).

5.3 | Eustatic Forcing and Autogenic Timing of Transgression

While eustatic sea-level rise determines the broader window within which transgression becomes possible, our results demonstrate that autogenic dynamics—particularly autoretreat—are often the primary mechanism governing the precise timing and spatial diachroneity of shoreline retreat across sedimentary basins. During the rise of RSL, the shoreline typically undergoes a transition from minor, rising-phase regression to transgression. This regression is autogenic in origin and differs fundamentally from the more extensive regression driven by falling sea level. Importantly, the timing of the transgressive shift is not determined solely by the rate of RSL rise, but also by the duration over which the RSL continues to rise. The delta must accumulate sufficient sediment and reach a critical size before transgression can initiate. Thus, the timescale of RSL rise is crucial, as it determines whether the delta system has enough time to fully develop this critical geometry. Muto and Steel (1997) proposed that changes in stratigraphic stacking patterns driven by autogenic mechanisms—such as transitions from progradation to retrogradation—become apparent only when the duration of external forcing (T) significantly exceeds the system's intrinsic timescale ($T >> \tau$; Muto and Steel 1997, 2004; Kim et al. 2006). This theoretical framework emphasises

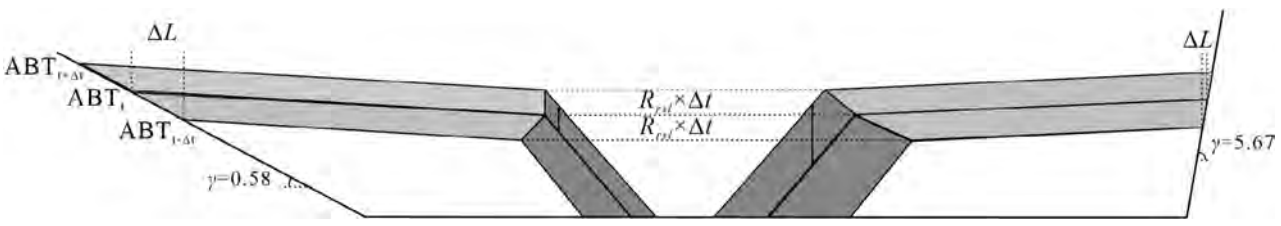

FIGURE 10 | Schematic diagram showing the change in sediment thickness due to slope effects. The black bidirectional arrows represent sediment thickness at time t for the following Δt. On the left side with a 0.58 slope, sediment thickness is equal to $R_{rsl}\times\Delta t$, at which point the shoreline stops advancing seaward. On the right side with a 5.67 slope, the sediment thickness is greater than $R_{rsl}\times\Delta t$, at which point the shoreline continues to advance seaward. ABT, alluvial–basement transition.

that the duration of RSL rise is a critical factor in determining whether a transgressive event occurs.

In basins with dual-provenance directions, three distinct scenarios arise depending on the timing of transgression initiation in different sedimentary systems (T_1, T_2, where $T_1 < T_2$) and the duration of RSL rise (T_{rsl}): (i) Short RSL Rise Duration ($T_{rsl} < T_1 < T_2$, Figure 11a): In this case, all fluvio-deltaic systems fail to reach the critical transgression threshold within such a short time, resulting in widespread regression across the basin. (ii) Intermediate RSL Rise Duration ($T_1 < T_{rsl} < T_2$, Figure 11b): One delta undergoes transgression while another continues to prograde, producing asymmetric stacking patterns. Such diachronous transgression, often attributed to variable sediment supply or tectonics (Jiang et al. 2005), may also arise from purely autogenic dynamics (Muto and Steel 1992; Wang et al. 2024). (iii) Long RSL Rise Duration ($T_1 < T_2 < T_{rsl}$, Figure 11c): When the RSL rise duration is long enough, the sedimentary systems across multiple provenance directions within the basin all experience a transition from regression to transgression.

The intrinsic timescale of a delta system (τ_{2D}) depends on sediment supply (q_s), shoreline slope, and RSL rise rate, and can be expressed as $\tau_{2D} \propto q_s / |R_{rsl}|^2$. For example, Wang et al. (2024) estimated τ for the Yangtze Delta to be ~1.338×10^3 years under modern high-supply and rapid RSL rise, but as large as 1.2×10^5 years under reduced Holocene supply and slower RSL change. These values suggest that asynchronous transgression within a single basin can occur on timescales of ~10^5 years (Paola 2016).

Eustatic fluctuations, driven by orbital forcing, operate on 10^4–10^5 years timescales (Lisiecki and Raymo 2005; Westerhold et al. 2020). These define the intervals during which transgression is possible. Within such intervals, however, the exact timing of shoreline turnaround and the development of concave retreat trajectories are governed by autogenic autoretreat. In summary, eustatic and autogenic controls are coupled in origin but decoupled in timing. Eustatic rise provides the necessary boundary condition for transgression, whereas autogenic processes dictate its local timing and spatial expression, producing significant diachroneity even under regionally uniform forcing. For lake-level fluctuations, however, these are not orbitally driven but are instead primarily influenced by catchment hydrology (Cardille et al. 2004; Somogyvári et al. 2024).

5.4 | Validating the Small-Scale Flume Tank Models Through Natural Example

In traditional sequence stratigraphy, progradation refers to regression, while retrogradation indicates transgression (Van Wagoner et al. 1990; Hannah 2004). This description may obscure spatiotemporal variations in transgression onset driven by sediment supply and basin slope—a limitation resolved by the Canterbury Plain case. Here, asynchronous shoreline responses to identical RSL rise (e.g., Waimakariri regression vs. Opihi transgression) demonstrate why progradation-retrogradation transitions cannot be treated as time-parallel boundaries. The Canterbury Plain, located on the east coast of New Zealand's South Island and divided by the North Banks Peninsula (Figure 12a,b), offers a valuable case study. Major rivers, such as the Waimakariri, Rakaia, Rangitata, and Ashburton, flow from west to east, and the area's shoreline dynamics are influenced by sea level, wave action, and coastal drift (Wilson 1985; Leckie 1994; Barnes 1995). During the Last Glacial Maximum (approximately 18,000 years ago), sea level was located at or slight beyond the continental shelf edge, reaching depths of up to 113 m (Jansen et al. 1979; Carter et al. 1986). As eustatic sea level rose for about 11,000 years, the shoreline advanced seaward, forming extensive alluvial river deltas, followed by transgressions when RSL began to rise from about 18,000 years ago (Muto and Wang 2024).

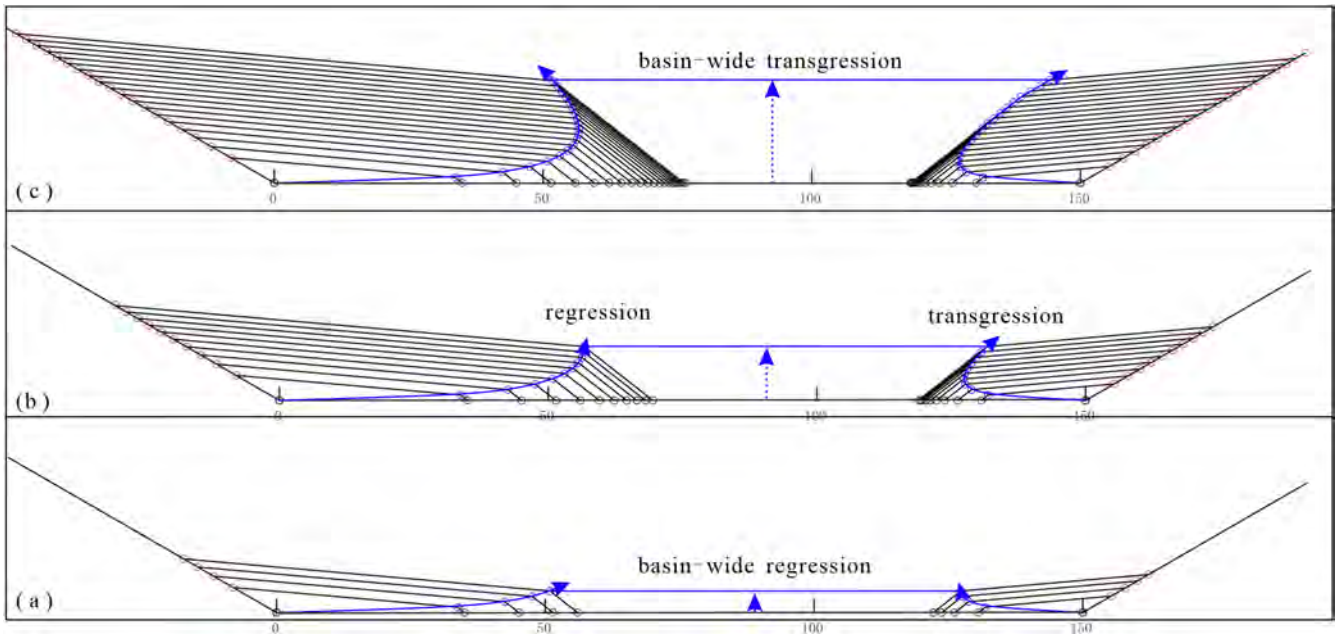

FIGURE 11 | The shoreline trajectories were influenced by different durations of RSL rise.

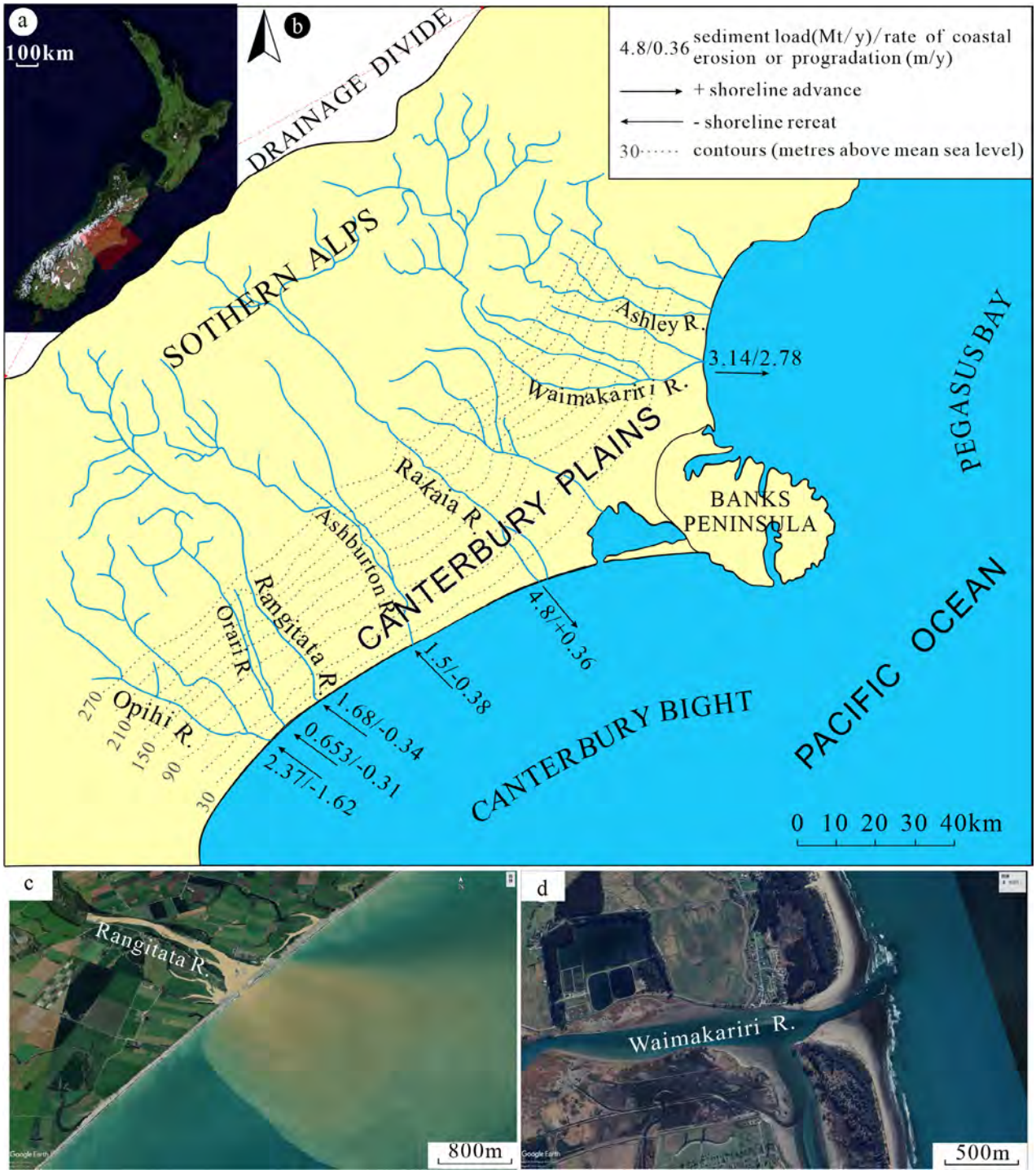

FIGURE 12 | Rate of coastal sediment load and rate of coastal erosion or progradation in the Canterbury Plains. (a) Geographical Location of New Zealand; (b) Rivers and Shorelines of the Canterbury Plains; (c) Subaqueous Sediment Deposition at the Mouth of the Rangitata River; (d) Small Delta at the Mouth of the Waimakariri River (b: Dates are from Wilson 1976; Gibb 1978; Basher et al. 1988 and Hicks et al. 2011. (a, c, d) *Source:* Google Earth.)

Over the 11,500 years following the last Ice Age (18,000–6500 years BP), eustatic sea level rose at an average rate of 0.01 m/year, approximately 10 times the current RSL rise rate (Carter et al. 1986; Fairbanks 1989). Concurrently, a warming climate change led to denser vegetation in river catchments, reducing sediment supply (Wilson 1985). The combination of rapid eustatic sea-level rise and lower sediment supply resulted in a smaller critical scale for transgression, causing river-delta systems to retreat landward, characteristic of non-deltaic transgressions (Wang and Muto 2024). The Christchurch Formation exemplifies this, as it records a marine transgression consisting of lagoonal, dune, coastal swamp, shell, and peat deposits overlying glacial outwash gravels, indicating that during the transition from the last glacial period to the Holocene, seawater rapidly advanced inland forming estuarine–lagoon–coastal environments, rather than typical deltaic deposits (Brown et al.

1988). From 1989 to 2000, the RSL rose at an average rate of 1.6×10^{-3} m/year, with no evidence of acceleration during this period (Hannah 2004). As the RSL rise rate decreases, the critical size for fluvio-deltaic systems increases. For example, in the Waimakariri River, with a sediment supply rate of 5.95 Mt/year, the shoreline advances seaward at a rate of 2 m/year, demonstrating delta regression (Hicks et al. 2011).

The influence of sediment transport rates on the timing of transgression is significant. On the southern peninsula, the Rakaia, Rangitata, and Ashburton Rivers have similar profile gradients (5×10^{-3}) and are influenced by strong wave action and coastal currents (Griffiths and Glasby 1985). The Rakaia River, with a sediment supply rate of 4.8 Mt/year, has a higher supply than the others, allowing the southern shoreline to advance at 0.3 m/year (Griffiths and Glasby 1985). In contrast, rivers with lower sediment supply rates, such as the Rangitata and Ashburton, experience varying rates of landward retreat.

Canterbury Bight, extending from Timaru to Banks Peninsula, is characterised by Pleistocene sediment-eroded cliffs behind a gravelly beach (Speight 1950; Gibb 1978). Physical simulations show that with a steep hinterland slope, RSL rise can cause the shoreline to transition from retreat to landward migration, ultimately leading to autodrowning. Rivers like the Opihi and Orari have low sediment supply rates, while coastal currents and strong wave action further transport sediment, reducing the effective accumulation of stratigraphic deposits, particularly along the southern bank of the Rakaia River (Leckie 1994, Figure 12). During flood periods, the estuarine turbidity maximum is observed in the Opihi River when sediment supply is high, providing evidence for transgression and eventual autodrowning (Figure 12c). In contrast, the Waimakariri River, with a sediment supply rate of 5.95 Mt/year and a hinterland slope of approximately 1×10^{-3} (Hicks et al. 2011), advances seaward in a deltaic regression pattern (Figure 12d). These examples demonstrate how slope and sediment supply rate affect the timing and stratigraphy of transgression.

6 | Conclusions

This study is based on two-dimensional experiments and establishes a dual-provenance stratigraphic model for sedimentary basin evolution under conditions of stable sediment supply and relative sea level (RSL) rise. The research demonstrates that the occurrence of transgression is not solely driven by sea level rise, but is also closely linked to the size of the river delta, sediment supply rate, RSL rise rate, and changes in the hinterland slope. The main conclusions are as follows:

1. The effects of sediment supply rate (q_s) and RSL rise rate (R_{rsl}) on transgression are similar. As sediment supply increases, the occurrence of transgression is delayed, whereas an increase in the relative sea level rise rate accelerates transgression. Both factors influence the timing of transgression by altering the size of the river delta system.
2. The occurrence of transgression is closely related to the size of the river delta system. Based on the autoretreat framework, this size represents the threshold where sediment supply can no longer offset accommodation creation during RSL rise. Transgression only occurs when the delta expands beyond this critical limit; until then, regression persists even under rising RSL. This critical size is jointly controlled by sediment supply rate, RSL rise rate, and hinterland slope.
3. Hinterland slope affects subaerial and subaqueous allocations of sediment. Steeper slopes result in less subaerial sediment accumulation and more subaqueous sediment accumulation. Steeper slopes reduce subaerial sediment allocation and increase subaqueous deposition. Consequently, the subaerial realm expands more slowly while the subaqueous realm aggrades more rapidly, which delays the onset of transgression. Under dimensionless conditions, the effect of slope on transgression is limited. However, for different sedimentary systems, considering the length and time scales determined by sediment supply rate and RSL rise rate, the impact of slope on transgression is amplified by several orders of magnitude.

This study provides a new theoretical framework for interpreting autogenic controls on transgression timing during relative sea-level rise, enabling more accurate reconstructions of paleoenvironments and offering theoretical support for basin modelling. Although the study is based on a two-dimensional experimental model with certain scale and parameter limitations, future research could deepen the understanding of the asynchronous mechanisms of transgression in sedimentary basins by incorporating three-dimensional analysis, expanding the range of sedimentary environments, and considering additional environmental variables.

Acknowledgements

We thank Ronald J. Steel, James H. Gearon, and an anonymous reviewer for their constructive comments and suggestions.

Funding

This study was supported in part by the National Natural Science Foundation of China (42172108), National Science and Technology Major Project (2025ZD1402707), the Institute of Geology and Geophysics of the CAS (THEMSIE04010101).

Conflicts of Interest

The authors declare no conflicts of interest.

Data Availability Statement

The data that support the findings of this study are available from the corresponding author upon reasonable request.

References

Barnes, P. M. 1995. "High-Frequency Sequences Deposited During Quaternary Sea-Level Cycles on a Deforming Continental Shelf, North Canterbury, New Zealand." *Sedimentary Geology* 97, no. 3: 131–156. https://doi.org/10.1016/0037-0738(94)00141-G.

Basher, L. R., D. M. Hicks, M. J. McSaveney, et al. 1988. "The Lower Waimakariri River Floodplain: A Geomorphological Perspective: Soil Conservation Group Report." Ministry of Works and Development, Christchurch, New Zealand, 33 p.

Brown, L. J., D. D. Wilson, N. T. Moar, and D. C. Mildenhall. 1988. "Stratigraphy of the Late Quaternary Deposits of the Northern Canterbury Plains, New Zealand." *New Zealand Journal of Geology and Geophysics* 31, no. 3: 305–335. https://doi.org/10.1080/00288306.1988.10417779.

Cardille, J., M. T. Coe, and J. A. Vano. 2004. "Impacts of Climate Variation and Catchment Area on Water Balance and Lake Hydrologic Type in Groundwater-Dominated Systems: A Generic Lake Model." *Earth Interactions* 8: 1–24. https://doi.org/10.1175/1087-3562(2004)8<1:IOCVAC>2.0.CO;2.

Carter, R. M., L. Carter, and D. P. Johnson. 1986. "Submergent Shorelines in the SW Pacific: Evidence for an Episodic Post-Glacial Transgression." *Sedimentology* 33, no. 5: 629–649. https://doi.org/10.1111/j.1365-3091.1986.tb01967.x.

Cazenave, A., and W. Llovel. 2010. "Contemporary Sea Level Rise." *Annual Review of Marine Science* 2: 145–173. https://doi.org/10.1146/annurev-marine-120308-081105.

Embry, A. F., and E. P. Johannessen. 1992. *T–R Sequence Stratigraphy, Facies Analysis and Reservoir Distribution in the Uppermost Triassic–Lower Jurassic Succession, Western Sverdrup Basin, Arctic Canada*. Vol. 2, 121–146. Norwegian Petroleum Society Special Publication.

Fairbanks, R. G. 1989. "A 17 000-Year Glacio-Eustatic Sea Level Record: Influence of Glacial Melting Rates on the Younger Dryas Event and Deep-Ocean Circulation." *Nature* 342, no. 6250: 637–642. https://doi.org/10.1038/342637a0.

Gearon, J. H., C. Olariu, and R. J. Steel. 2022. "The Supply-Generated Sequence: A Unified Sequence-Stratigraphic Model for Closed Lacustrine Sedimentary Basins With Evidence From the Green River Formation, Uinta Basin, Utah, U.S.A." *Journal of Sedimentary Research* 92, no. 9: 813–835. https://doi.org/10.2110/jsr.2021.096.

Gibb, J. G. 1978. "Rates of Coastal Erosion and Accretion in New Zealand." *New Zealand Journal of Marine and Freshwater Research* 12, no. 4: 429–456. https://doi.org/10.1080/00288330.1978.9515770.

Griffiths, G. A., and G. P. Glasby. 1985. "Input of River-Derived Sediment to the New Zealand Continental Shelf: I. Mass." *Estuarine, Coastal and Shelf Science* 21, no. 6: 773–787. https://doi.org/10.1016/0272-7714(85)90072-1.

Hannah, J. 2004. "An Updated Analysis of Long-Term Sea Level Change in New Zealand." *Geophysical Research Letters* 31: L03307. https://doi.org/10.1029/2003GL019166.

Haq, B. U., J. Hardenbol, and P. R. Vail. 1987. "Chronology of Fluctuating Sea Levels Since the Triassic." *Science* 235, no. 4793: 1156–1167. https://doi.org/10.1126/science.235.4793.1156.

Hicks, M., U. Shankar, A. Mckerchar, et al. 2011. "Suspended Sediment Yields From New Zealand Rivers." *Journal of Hydrology. New Zealand* 50: 81–142.

Jansen, J. H. F., T. C. E. van Weering, and D. Eisma. 1979. "Late Quaternary Sedimentation in the North Sea." In *The Quaternary History of the North Sea*, 175–187. Upsala University.

Jiang, Z., H. Lu, W. Yu, Y. Sun, and D. Guan. 2005. "Transformation of Accommodation Space of the Cretaceous Qingshankou Formation, the Songliao Basin, NE China." *Basin Research* 17, no. 4: 569–582. https://doi.org/10.1111/j.1365-2117.2005.00275.x.

Johnson, J. G., G. Klapper, and C. A. Sandberg. 1985. "Devonian Eustatic Fluctuations in Euramerica." *Geological Society of America Bulletin* 96, no. 5: 567. https://doi.org/10.1130/0016-7606(1985)96<567:DEFIE>2.0.CO;2.

Kim, W., C. Paola, V. R. Voller, and J. B. Swenson. 2006. "Experimental Measurement of the Relative Importance of Controls on Shoreline Migration." *Journal of Sedimentary Research* 76, no. 2: 270–283. https://doi.org/10.2110/jsr.2006.019.

Le Hooke, R. B., and W. L. Rohrer. 1979. "Geometry of Alluvial Fans: Effect of Discharge and Sediment Size." *Earth Surface Processes* 4, no. 2: 147–166. https://doi.org/10.1002/esp.3290040205.

Leckie, D. A. 1994. "Canterbury Plains." *New Zealand—Implications for Sequence Stratigraphic Models: AAPG Bulletin* 78, no. 8: 1240–1256. https://doi.org/10.1306/A25FEABD-171B-11D7-8645000102C1865D.

Lisiecki, L. E., and M. E. Raymo. 2005. "A Pliocene-Pleistocene Stack of 57 Globally Distributed Benthic $\delta^{18}O$ Records." *Paleoceanography* 20, no. 1: PA1003. https://doi.org/10.1029/2004PA001071.

Mastronuzzi, G., P. Sansò, C. V. Murray-Wallace, and I. Shennan. 2005. "Quaternary Coastal Morphology and Sea-Level Changes—An Introduction." *Quaternary Science Reviews* 24, no. 18: 1963–1968. https://doi.org/10.1016/j.quascirev.2005.06.001.

Milne, G. A., W. R. Gehrels, C. W. Hughes, and M. E. Tamisiea. 2009. "Identifying the Causes of Sea-Level Change." *Nature Geoscience* 2, no. 7: 471–478. https://doi.org/10.1038/ngeo544.

Muto, T. 2001. "Shoreline Autoretreat Substantiated in Flume Experiments." *Journal of Sedimentary Research* 71, no. 2: 246–254. https://doi.org/10.1306/091400710246.

Muto, T., R. Furubayashi, A. Tomer, et al. 2016. "Planform Evolution of Deltas With Graded Alluvial Topsets: Insights From Three-Dimensional Tank Experiments, Geometric Considerations and Field Applications." *Sedimentology* 63, no. 7: 2158–2189. https://doi.org/10.1111/sed.12301.

Muto, T., and H. Okada. 1991. "A Comment on Modelling the Paleogeography of Confined and Unconfined Marine Gilbert-Type Deltas." *Cuadernos de Geologia Lberica* 15: 139–161.

Muto, T., and R. J. Steel. 1992. "Retreat of the Front in a Prograding Delta." *Geology* 20, no. 11: 967–970. https://doi.org/10.1130/0091-7613(1992)020<0967:ROTFIA>2.3.CO;2.

Muto, T., and R. J. Steel. 1997. "Principles of Regression and Transgression; the Nature of the Interplay Between Accommodation and Sediment Supply." *Journal of Sedimentary Research* 67, no. 6: 994–1000. https://doi.org/10.1306/D42686A8-2B26-11D7-8648000102C1865D.

Muto, T., and R. J. Steel. 2004. "Autogenic Response of Fluvial Deltas to Steady Sea-Level Fall: Implications From Flume-Tank Experiments." *Geology* 32, no. 5: 401–404. https://doi.org/10.1130/G20269.1.

Muto, T., R. J. Steel, and J. B. Swenson. 2007. "Autostratigraphy: A Framework Norm for Genetic Stratigraphy." *Journal of Sedimentary Research* 77, no. 1: 2–12. https://doi.org/10.2110/jsr.2007.005.

Muto, T., and J. Wang. 2024. "Autogenic Shrinkage and Channel Destabilization of an Overexpanded Downstream Alluvial System Under Steady Rise of Relative Sea Level: An Experimental Study." *Earth and Planetary Science Letters* 637: 118722. https://doi.org/10.1016/j.epsl.2024.118722.

Osman, A., R. J. Steel, R. Ramsook, and C. Olariu. 2024. "Impact of Wave, Tides and Fluid Mud on Fluvial Discharge Across a Compound Clinoform (Pliocene Orinoco Delta)." *Sedimentology* 71, no. 4: 1113–1148.

Paola, C. 2016. "A Mind of Their Own: Recent Advances in Autogenic Dynamics in Rivers and Deltas." In *Autogenic Dynamics and Self-Organization in Sedimentary Systems, SEPM Special Publication*, vol. 106, 5–17. SEPM (Society for Sedimentary Geology).

Paola, C., K. M. Straub, D. Mohrig, and L. Reinhardt. 2009. "The "Unreasonable Effectiveness" of Stratigraphic and Geomorphic Experiments in Earth-Surface Science." *Science* 326, no. 5960: 578–581.

Patruno, S., G. J. Hampson, and C. A. L. Jackson. 2015. "Quantitative Characterisation of Deltaic and Subaqueous Clinoforms." *Earth-Science Reviews* 142: 79–119. https://doi.org/10.1016/j.earscirev.2015.01.004.

Petter, A. L., and T. Muto. 2008. "Sustained Alluvial Aggradation and Autogenic Detachment of the Alluvial River from the Shoreline in

Response to Steady Fall of Relative Sea Level." *Journal of Sedimentary Research* 78, no. 2: 98–111. https://doi.org/10.2110/jsr.2008.012.

Rey, F. M., C. Olariu, and R. J. Steel. 2022. "Using the Modern Colorado Delta to Reconstruct the Compound Clinoforms of the Pliocene Colorado Delta." *Journal of Sedimentary Research* 92, no. 5: 405–432. https://doi.org/10.2110/jsr.2021.098.

Shanley, K. W., and P. J. McCabe. 1994. "Perspectives on the Sequence Stratigraphy of Continental Strata." *AAPG Bulletin* 78, no. 4: 544–568.

Somogyvári, M., D. Scherer, F. Bart, U. Fehrenbach, A. Okujeni, and T. Krueger. 2024. "A Hybrid Data-Driven Approach to Analyze the Drivers of Lake Level Dynamics." *Hydrology and Earth System Sciences* 28: 4331–4348. https://doi.org/10.5194/hess-28-4331-2024.

Speight, R. 1950. "An Eroded Coastline." *Transactions and Proceedings of the Royal Society of New Zealand* 78: 3–13.

Steel, R. J., A. Osman, V. M. Rossi, et al. 2024. "Subaqueous Deltas in the Stratigraphic Record: Catching Up With the Marine Geologists." *Earth-Science Reviews* 256: 104879. https://doi.org/10.1016/j.earscirev.2024.104879.

Summerhayes, C. P. 1986. "Sealevel Curves Based on Seismic Stratigraphy: Their Chronostratigraphic Significance: Palaeogeography." *Palaeoclimatology, Palaeoecology* 57, no. 1: 27–41. https://doi.org/10.1016/0031-0182(86)90004-0.

Thomas, W., M. Norbert, J. D. Anna, et al. 2020. "An Astronomically Dated Record of Earth's Climate and Its Predictability Over the Last 66 Million Years." *Science* 369, no. 6509: 1383–1387. https://doi.org/10.1126/science.aba6853.

Tomer, A., and T. Muto. 2010. "Emergence and Drowning of Fluviodeltaic Systems During Steady Rise of Sea Level: Implication From Geometrical Modeling and Tank Experiments." *Journal of the Sedimentological Society of Japan* 69: 63–72.

Tomer, A., T. Muto, and W. Kim. 2011. "Autogenic Hiatus in Fluviodeltaic Successions: Geometrical Modeling and Physical Experiments." *Journal of Sedimentary Research* 81: 207–217.

Vail, P. R., R. M. Mitchum, and S. Thompson III. 1977. "Seismic Stratigraphy and Global Changes of Sea Level, Part 3: Relative Changes of Sea Level From Coastal Onlap." In *Seismic Stratigraphy—Applications to Hydrocarbon Exploration*, vol. 26, 63–81. AAPG Memoirs.

Van De Lageweg, W. I., and A. B. A. Slangen. 2017. "Predicting Dynamic Coastal Delta Change in Response to Sea-Level Rise, 2." *Journal of Marine Science and Engineering* 5, no. 2: 24. https://doi.org/10.3390/jmse5020024.

Van Wagoner, J. C., R. M. Mitchum, K. M. Campion, and V. D. Rahmanian. 1990. *Siliciclastic Sequence Stratigraphy in Well Logs, Cores, and Outcrops: Concepts for High-Resolution Correlation of Time and Facies. Methods in Exploration Series Volume 7*, 55. American Association of Petroleum Geologists.

Van Wagoner, J. C., H. W. Posamentier, R. M. Mitchum, et al. 1988. *An Overview of Sequence Stratigraphy and Key Definitions. In: Sea Level Changes – An Integrated Approach*. Vol. 42, 39–45. SEPM Special Publication.

Wang, J., and T. Muto. 2021. "Autostratigraphic Modelling of the Growth of Alluvial-Shelf Systems During Steady Base-Level Cycles: Two-Dimensional Tank Experiments." *Sedimentology* 68, no. 1: 135–167. https://doi.org/10.1111/sed.12789.

Wang, J., and T. Muto. 2024. "The Intrinsic Rarity of Equilibrium Response in Stratigraphic Processes." *Geosystems and Geoenvironment* 3: 100281. https://doi.org/10.1016/j.geogeo.2024.100281.

Wang, J., T. Muto, and B. Xian. 2024. "Large-Scale Autogenic Stratigraphic Mechanisms and Autostratigraph." *Acta Geologica Sinica* 98, no. 7: 1977–2000. https://doi.org/10.19762/j.cnki.dizhixuebao.2023164.

Wang, J., H. Naruse, and T. Muto. 2020. "The Grade Index Model as a Rationale for Autogenic Nonequilibrium Responses of Deltaic Clinoform to Relative Sea-Level Rise." *Basin Research* 32, no. 2: 378–387. https://doi.org/10.1111/bre.12418.

Westerhold, T., N. Marwan, A. J. Drury, et al. 2020. "An Astronomically Dated Record of Earth's Climate and its Predictability Over the Last 66 Million Years." *Science* 369: 1383–1387. https://doi.org/10.1126/science.aba6853.

Wilson, D. D. 1976. "Hydrogeology of Metropolitan Christchurch." *Journal of Hydrology. New Zealand* 15, no. 2: 101–120.

Wilson, D. D. 1985. "Erosional and Depositional Trends in Rivers of the Canterbury Plains." *New Zealand: Journal of Hydrology (New Zealand)* 24, no. 1: 32–44.

Withjack, M., R. Schlische, and P. Olsen. 2002. "Rift Basin Structure and Its Influence on Sedimentary Systems." *SEPM Special Publication* 73: 57–82. https://doi.org/10.2110/pec.02.73.0057.

Zhong, G. 2008. *Late Cenozoic Seismic Onlap-Offlap Sequences and Sea Level Changes on the Northern Sunda Shelf, South China Sea*. Tongji University.